DRFC/CAD

EUR-CEA-FC-1334

Numerical modelisation of RF waves in the ion cyclotron range of frequency for Tokamak plasmas

D. EDERY, H. PICQ, A. SAMAIN, D.J. GAMBIER

Décembre 1987

ASSOCIATION EURATOM-C.E.A
DEPARTEMENT DE RECHERCHES SUR LA FUSION CONTROLEE
C.E.N./CADARACHE
13108 SAINT PAUL LEZ DURANCE CEDEX

Numerical modelisation of RF waves in the ion cyclotron range of frequency for Tokamak plasmas

D. EDERY, H. PICQ, A. SAMAIN, D.J. GAMBIER

Numerical modelisation of RF waves in the ion cyclotron range of frequency for Tokamak plasmas

D. EDERY, H. PICQ[1], A. SAMAIN, D.J. GAMBIER

Association Euratom CEA sur la Fusion

CEN Cadarache, 13108 St Paul Lez Durance France

[1] CISI-Ingénierie, CEN Cadarache, B.P.1

13115 St Paul Lez Durance France

ABSTRACT

The purpose of this paper is to present the numerical code ALCYON developed to compute the RF field structure in the ion cyclotron range of frequencies. The code handles fundamental and second harmonic heating while the mode conversion onto modes of decreasing wavelength is simulated by a selective power absorption on slow waves when their wavelength reaches the mesh size.

I Introduction

The problem of calculating the structure of Ion Cyclotron Range of Frequency waves (ICRF) has become crucial in present day Tokamaks as it plays an important role in coupling the heating power [1]. A variational method , developed in a previous article [2], answers the question of the ICRF wave equations in hot Tokamak plasmas, but so far no numerical code, based on this derivation, was constructed. The purpose of this paper is then to present the numerical code "ALCYON" specially developed to compute the structure of the ICRF field and the power deposited in the Tokamak plasma in practical RF heating scenarios.

The variational principle given in [2], is equivalent to the full set of Maxwell and Vlasov equations and goes beyond the limitation of the WKB approximation, taking into account the actual structure of the RF field. To escape from the WKB approach may appear at first sight, unnecessary in large Tokamaks in view of the relatively small tranverse wavenumber (ω/c_A) of the magnetosonic wave, which constitutes the background structure of the ICRF field. However many difficulties arise as soon as, the inhomogeneity along the flux lines, the mode conversion process and the stochasticity of the ray trajectories are to be introduced.

Considering first the inhomogeneity, the WKB method ignores the problem of the variation of $\nabla_{//}\omega_c$ in the resonant process and the broadening of the cyclotron resonance is always determined by its Doppler value $K_{//}v_{//}$. This leads to a misestimation if $K_{//}v_{//} < |v_{//}\nabla_{//}\omega_c|^{1/2}$, the latter quantity being the "ballistic" [3] broadening of the cyclotron resonance , reflecting that the ion cross the resonance over a finite time $\simeq |v_{//}\nabla_{//}\omega_c|^{-1/2}$.

On the other hand, the constraint $\nabla K_\perp << K_\perp^2$ imposed by WKB is never satisfied in the vicinity of the mode conversion layer. Indeed in this domain, the ICRF wave presents a point of resonance ($K_\perp \to \infty$), a cutoff ($K_\perp \to 0$) and a turning point ($dK_\perp/dx \to \infty$) at which this constraint is violated. The linear mode conversion of the magnetosonic wave into waves of decreasing wavelength has been investigated by many authors [4] .While the representation of the RF field in independent WKB waves is no longer possible within the mode conversion layer, there exists a set of connecting formulas [5] , which allows to link the asymptotic WKB solutions on both sides of the conversion zone and which permits to estimate the power carried away by the converted waves. It is also often proposed that the effect of mode conversion can be correctly represented by introducing an arbitrary antihermitian part in the dielectric tensor [6] . This procedure eliminates the singularity problem and allows to derive the energy transferred through the converted waves. It is justified by the following physical idea : waves generated at the mode conversion exhibit a wavelength decreasing rapidly so that they loose coherence with the mother magnetosonic wave; therefore they have no feedback action on the latter and may safely be damped by artificial means.

The WKB method may also be limited by the topology of ray trajectories. In configurations where rays are stochastic, two trajectories emerging from two nearby points ($\vec{x}$, $\vec{K}$) diverge exponentially. In such conditions, the usual WKB phase expression $\int K\,dx$ may produce a complex phase structure from one ray to another, which, if it appears with a scale < K^{-1}, disqualifies the WKB calculations. This effect occurs in the absence of effective damping of the waves, allowing the excitation of all wave numbers compatible with the dispersion relation. It has been suggested that the lower hybrid current drive "gap problem" may be explained by this stochastic behaviour. A numerical approach taking into account the exact RF field structure and not referring to the WKB approximation is of general interest in such context.

Among the several existing full wave codes [7,8,9], the code LION [9] has properly simulated the propagation and absorption of the magnetosonic wave, as well as torsional resonances. It uses the cold plasma response in the full Tokamak geometry, adding a simple antihermitian term to the dielectric tensor to suppress the conversion singularity. However the $\nabla_{//}\omega_c$ influence on the resonant absorption is ignored. On the other hand, the artificial damping term is not selective for the high K components of the field, as desirable. Then it is not guaranteed that it leads to a correct representation of the decorrelation between the small scale converted waves and the magnetosonic field.

The originality of the "ALCYON" code we present here is to include the $\nabla_{//}\omega_c$ effect, the finite Larmor radius effects leading to second harmonic resonance and conversion into Bernstein waves, and an artificial damping mechanism to simulate the conversion process which is highly selective on high K components. Finite element discretisation is used in the radial direction and Fourier transform in the poloidal direction.

In the next section we will shortly present the physics that the code handles, namely we will review the resonance and conversion phenomenons and will establish their consequences on the code organisation. In sect. III we will describe the signifiance of the functional forms that have been implemented, while in sect. IV the numerical stability problem will be analysed . Finally in sect.V, outputs of the code in typical ICRF conditions will be presented.

II ICRF waves structure and numerical implications

In this section we review the properties of the RF field in the ion cyclotron range, in order to specify the set of constraints that must be implemented in the numerical code.

Generally, the perturbed electromagnetic field is formed of an Alfven compressional magnetosonic mode which is susceptible of generating torsional and electrostatic modes if a mode conversion process occurs. It is only the large scale Alfven compressional field that is involved in the present modelisation. This field propagates energy from an antenna throughout the plasma, its direction of propagation is mainly across the magnetic lines and its velocity is of the order of the Alfven velocity C_A. Obviously the first constraint for the code is that the number of mesh points be large enough, to cope with the bulk scale $K_\perp^{-1} \simeq (\omega/C_A)^{-1}$ of the compressional field. A characteristic property of the compressional mode comes from the very low parallel impedance of the plasma forcing the electric perturbation $\delta\vec{E}$ to be tranverse to the equilibrium magnetic field. Taking advantage of the Tokamak axisymetry in the toroidal direction φ, we express the electric and magnetic RF components to be handled by the code as:

$$
\begin{aligned}
\delta\vec{E} &= -\frac{\partial}{\partial t}(\,\delta\vec{A}\,) \\
\delta\vec{B} &= \vec{\nabla}\times(\delta\vec{A}) \\
\delta\vec{A} &= \vec{A}(\psi,\theta,\varphi)\ \exp(i\omega t) + c.c. \qquad (1) \\
\tilde{\vec{A}}(\psi,\theta,\varphi) &= A_1(\psi,\theta)e^{iN\varphi}\ \vec{e}_\psi + A_2(\psi,\theta)e^{iN\varphi}\ \vec{e}_\theta
\end{aligned}
$$

where ψ and θ are respectively the coordinate of the poloidal flux embraced by each magnetic surface and the angular coordinate along each surface ψ. The set of vectors $\vec{e}_\psi, \vec{e}_\theta$ are the unit tranverse vectors normal and tangent to the precedent ψ-surface.

The field may be in resonance with an ion species in cyclotron resonance layers located near surfaces where $\omega+p\omega_c=0$, with $\omega_c(\psi,\theta)=-eB/m$. The ions gain perpendicular energy during their transit in the cyclotron layer from their interaction with the component δE_c of δE rotating in the ion direction [10,11]. In fact, a consequence of the resonance is a very low impedance for the component δE_c, which may then be strongly attenuated within the layer. It is essential for the code to be capable of calculating precisely that field structure as it rules the power gained by the particles. This means that the code must cope with the width of the cyclotron resonace layer, defined as [2]:

$$|\omega + p\omega_c| \ll \delta\omega_c$$

$$\delta\omega_c = \mathrm{Max}\left\{\frac{N}{R}v_{th},\ \sqrt{v_{th}\nabla_{//}(p\omega_c)}\right\};\quad v_{th} = \sqrt{\frac{2T}{m}}$$

where $(N/R)v_{th}$ accounts for the traditional Doppler effect, while the expression $|v_{th}\nabla_{//}(p\omega_c)|^{1/2}$ is characteristic of the transit time τ during which a variation $\delta(p\omega_c)\simeq 1/\tau$ takes place ($\delta(p\omega_c)\simeq\tau\ v_{th}\nabla_{//}(p\omega_c)\simeq 1/\tau\ \simeq\ |v_{th}\nabla_{//}(p\omega_c)|^{1/2}$). This constraint does not apply if the density of resonant particles is very small: the condition for the resonant structure of the field in the cyclotron layer to be ignorable is expressed as:

$$|\ (k_\perp\rho_c)^{2(|p|-1)}\omega_p^2\ |_{res} \ll \omega_p^2{}_{bulk}\frac{\delta\omega_c}{\omega_{c_{bulk}}} \tag{2}$$

where $\omega_p^2 = ne^2/m\varepsilon_0$, $\rho_c = v_{th}/\omega_c$, "res" and "bulk" referring to resonant and bulk ion particles respectively.

Another class of resonances which may be experienced by the compressional Alfven wave consists of the mode conversions onto waves of larger $K_\perp$[10,11,12]. The simplest mode conversion process takes place when the compressional wave is converted into torsional Alfven waves. The latter are localized on a given magnetic surface ψ with a poloidal structure K_{pol} in θ, defined by:

$$P(\psi,\theta,K_{//}) = 0$$

$$\text{where}\ \ P = \frac{\omega^2}{c^2} - K_{//}^2 - \sum_s \frac{\omega_{ps}^2}{c^2}\frac{\omega^2}{\omega^2 - \omega_{cs}^2} \tag{3}$$

$$\text{and}\ K_{//} = \frac{N}{R} + K_{pol}\frac{B_{pol}}{|\vec{B}|}$$

In the plasma bulk this relation implies for $K_{//}$ to be of the order of ω/C_A which corresponds to a value of $K_{pol} \simeq \frac{\omega}{C_A}\frac{B}{B_{pol}}$ much larger than $K_{pol} \simeq \frac{\omega}{C_A}$ typical of the compressional field. However, near the surface $P(\psi,\theta,K_{//}=N/R)=0$ the torsional field exhibits a smaller K_{pol} compatible with the compressional field. It is near this surface that the conversion takes place. Two different situations may then be encountered (Fig.1). Along its propagation, either the torsional wave runs into a cyclotron resonance, or it does'nt. In the first case the torsional wave energy is simply damped by the thermal ion motion at the location of the cyclotron resonance. In the second case a stationary eigenmode along θ may develop, of which the radial structure is determined by the Larmor radius effect.

Near a second harmonic resonance surface $\omega-2\omega_c(\psi,\theta)=0$, the magnetosonic wave may undergo a mode conversion into a slow ion Bernstein wave (Fig.2). The propagation of the ion Bernstein wave is mainly perpendicular to the magnetic ψ surfaces. Near the conversion surface its structure is again defined by $P(\psi,\theta,K_{//})=0$, but P includes now an additional term $\simeq \frac{\omega_p^2}{2c^2} K_\perp^2 \, \varrho_c^2 \, \frac{\omega^2}{\omega^2-4\omega_c^2}$ reflecting the finite Larmor radius effect enhanced by the proximity of the resonance $\omega-2\omega_c(\psi,\theta)=0$. The mode conversion is effective if this additional term, calculated with the magnetosonic $K_\perp$, is large enough so that the surface $P(\psi,\theta,K_{//}=N/R)=0$ lies out of the cyclotron layer. This occurs when the reversed inequality (2) with $p = 2$ is satisfied.

The effect of mode conversion leads to the developement of a sequence of field components with smaller and smaller scales. Of course, these components (ultimately the converted waves of increasing K) cannot be handled numerically. However they are less and less coupled to the primary magnetosonic wave. The latter is still safely computed if the set of decreasing scales is truncated by introducing in the numerics a selective damping acting on the smaller scales. Finally we may sum up the set of constraints that have to be implemented in the code: (i) the mesh must be sufficiently closed up to follow the magnetosonic wavenumbers ; (ii) it needs to be refined in the region of resonance; (iii) a functional form must be implemented to selectively cancel out modes of radial structure reaching the mesh size.

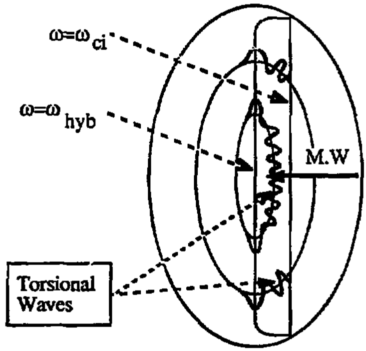

Figure 1
Torsional waves converted from the magnetosonic wave (M.W.) at the surface $\omega=\omega_{hyb}$.

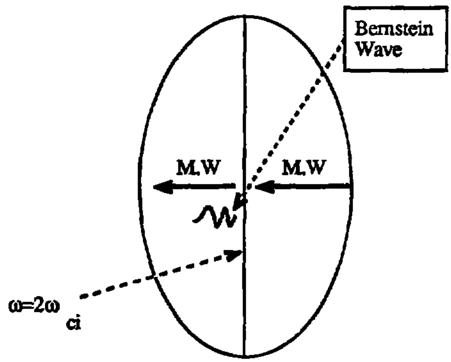

Figure 2
conversion into Bernstein wave near the second harmonic resonance $\omega=2\omega_{ci}$.

III Variational modelisation of the ICRF problem

Starting from the potential vector $\vec{A}$ in eq.1, through the set of Maxwell's equations a current $\vec{J}_M$ is produced. It is derived from $\vec{A}$ by the application of a linear operator $T_M(\vec{A})=\vec{J}_M$. The field $\vec{A}$ linearly perturbs the particle trajectories of each species and thereby produces a current $\vec{J}_P$ again derived through the application of a linear operator $T_P(\vec{A})=\vec{J}_P$. The field equation may then be written everywhere as:

$$\vec{J}_P - \vec{J}_M + \vec{J}_{Ant} = \vec{0}$$

or equivalently

$$T_P(\vec{A}) - T_M(\vec{A}) + \vec{J}_{Ant} = \vec{0}$$

where $\vec{J}_{Ant}(\psi,\theta)\ e^{i(\omega t+N\Phi)} + c.c.$ is the current density flowing in the antenna system, assumed to be known in the problem. From this constitutive relation the problem is given a convenient variational form built upon the functional form:

$$\mathcal{L}(\vec{A},\vec{A}^*) = \mathcal{L}_{Part}(\vec{A},\vec{A}^*) + \mathcal{L}_{Vac}(\vec{A},\vec{A}^*) - \mathcal{L}_{Ant}(\vec{A}^*)$$

$\mathcal{L}_{Ant}$ is a linear form in $\vec{A}^*$ reflecting the antenna:

$$\mathcal{L}_{Ant} = \mu_0 \iiint d_3\vec{x}\ \vec{J}_{Ant}(\vec{x}) . \vec{A}^*$$

and $\mathcal{L}_{Part}$, $\mathcal{L}_{Vac}$ are the bilinear forms in $\vec{A},\vec{A}^*$:

$$\mathcal{L}_{Vac}(\vec{A},\vec{A}^*) = \mu_0 \iiint d_3\vec{x}\ T_M(\vec{A}) . \vec{A}^* = \iiint d_3\vec{x} \left[\ |\vec{\nabla}\times\vec{A}|^2 - \frac{\omega^2}{c^2}|\vec{A}|^2 \right]$$

$$\mathcal{L}_{Part}(\vec{A},\vec{A}^*) = -\mu_0 \iiint d_3\vec{x}\ [\ T_p(\vec{A}) . \vec{A}^*\ ]$$

reflecting the Maxwell's equations and the plasma response, respectively. The field equations are then expressed in an equivalent manner by stating that the functional form $\mathcal{L}(\vec{A},\vec{A}^*)$ is extremum in $\vec{A}^*$. The power absorbed in the plasma is derived through the expression:

$$\mathcal{W} = \frac{2\omega}{\mu_o} \Im m(\mathcal{L}_{Part}) \tag{4}$$

One notes that $\mathcal{L}_{Vac}$ is real, so that, in the absence of power absorption, the functional form $\mathcal{L}_{Vac} + \mathcal{L}_{Part}$ reflecting the cavity response is real hermitian. The principle $\partial\mathcal{L}/\partial A^*=0$ implies that $\mathcal{L}=0$, so that $\mathcal{W} = 2\omega/\mu_0 \Im m(\mathcal{L}_{Ant})$. The plasma contribution Z to the antenna impedance is given by $Z=\frac{-i2\omega\mathcal{L}_{Ant}}{\mu_o|I|^2}$ where $I \exp(i\omega t)$ + c.c. is the RF current flowing in the antenna.

The difficulty is naturally to derive a manageable expression for $\mathcal{L}_{Part}$. The general approach followed in [2] is to take advantage of the integrability of unperturbed trajectories in the Tokamak magnetic configuration. The quasilinear perturbation of the trajectories is then formulated within the Hamiltonian formalism . One finds in the ICRF case for a given species the general expression of $\mathcal{L}_{Part}$

$$\mathcal{L}_{Part} = \mu_o \iiint d_3\vec{x} \sum_p \frac{n}{T} \langle R_p(v_\perp v_{//}, \vec{x})\rangle_{\vec{x}} \frac{\omega}{\omega+p\omega_{cs}(\vec{x})-i(+0)} \tag{5}$$

where $n(\vec{x})$, $T(\vec{x})$, $\omega_c(\vec{x})$ are respectively the density, temperature and cyclotron frequency of the species at each point $\vec{x}$. Furthermore $\langle . \rangle_{\vec{x}}$ designates the Maxwellian averaging at each point $\vec{x}$.

All the detailed information on the dispersive properties of the plasma are included in the expression of R_p. For each species, it is found that R_p is proportional to the integral along the particle trajectory of the perturbed Hamiltonian, and more precisely of its Fourier component H_p over the cyclotronic phase Φ_c, defined by:

$$- e\vec{v}_\perp . \vec{A}(\psi,\theta,\varphi) = \sum_p H_p(v_\perp, \vec{x}_G) \exp(ip\Phi_c)$$

where $v_\perp, v_{//}$, $\vec{x}_G$ constitute the usual set of slow dynamical variables, which together with the cyclotron phase Φ_c describe the phase space for the considered species. We then have:

$$R_p(v_\perp, v_{//}, \vec{x}) = \left| \frac{p v_{//} \nabla_{//} \omega_c}{2\pi} \right| \left| \int_{-\infty}^{+\infty} d\tau \, H_p(v_\perp, \vec{x} + \vec{v}_{//}\tau) \exp(ipv_{//}\nabla_{//}\omega_c \frac{\tau^2}{2}) \right|^2 \qquad (6)$$

The function R_p averages the value of $\vec{A}(\psi, \theta, \varphi)$ over a longitudinal distance λ which is the result of two competitive effects: the ω_C inhomogeneity along the field lines through the exponentional function and the longitudinal variations of the compressional field through H_p. This distance represents the longitudinal scalelength of the plasma dispersive properties linked with the resonance $\omega + p\omega_C = 0$.

It is found that, if the Doppler width $K_{//}v_{th}$ is much larger than the ballistic width $(v_{th}\nabla_{//} p\omega_c)^{1/2}$, then $K_{//}\lambda \gg 1$ and the field is susceptible of a WKB decomposition in terms proportional to $\exp(iK_{//}x_{//})$. In that case, integrating eq.(6) by the stationary phase technique, the R_p value reduces to:

$$R_p(v_\perp, v_{//}, \vec{x}) = |H_p(v_\perp, \vec{x} + \vec{v}_{//}\tau)|^2 \quad , \ \tau = -\frac{K_{//}}{p\nabla_{//}\omega_c}$$

an expression which, when introduced in (5), is leading to the usual Landau structure:

$$\mathcal{L}_{Part} = \mu_o \sum_p \iiint \frac{n}{T} \, |H_p(v_\perp, \vec{x})|^2 \left\langle \frac{1}{\omega + p\omega_c(\vec{x}) + K_{//}v_{//}} \right\rangle d_3\vec{x}$$

Furthermore when the H_p coefficients are Fourier decomposed over the poloidal angle θ,

$$H_p(v_\perp, \vec{x}) = \sum_m H_{pm}(\psi) \exp(im\theta) \exp(iN\varphi)$$

the expression of $\mathcal{L}$ takes the final form:

$$\mathcal{L}_{Part} = \mu_o \sum_p \sum_{m,m'} \int H_{pm} H^*_{pm'} D_{m,m'} d\psi \qquad (7)$$

$$D_{m,m'} = \int_0^{2\pi} J \left\langle \frac{1}{\omega + p\omega_c(\psi,\theta) + K_{//}v_{//}} \right\rangle \exp[i(m-m')\theta]\, 2\pi d\theta$$

$$J = d_3x/(d\psi d\theta d\varphi)$$

On the contrary if, owing to the inhomogeneity effect, the Doppler width $K_{//}v_{th}$ is not much larger than the width $(v_{th}\nabla_{//}p\omega_c)^{1/2}$ then the representation in independent waves varying as $\exp(iK_{//}x_{//})$ is no longer applicable. The analytical formula for $\mathcal{L}_{Part}$ continues to be of the form (7) but $D_{m,m'}$ is now given by:

$$D_{m,m'} = \int_0^{2\pi} J \left\langle \frac{1}{\omega + p\omega_c(\psi,\theta) + \frac{B_\phi}{RB}\left(N + \frac{m-m'}{2q}\right)v_{//}} \right\rangle \exp[i(m-m')\theta]\, 2\pi d\theta$$

where q is the safety factor.An approximate expression of $D_{m,m'}$ more suitable for computer handling has been implemented in the code, its expression being:

$$D_{m,m'} = \left[\int_0^{2\pi} J \left\langle \frac{1}{\omega + p\omega_c(\psi,\theta) + \frac{NB_\phi}{RB}v_{//}} \right\rangle \exp[i(m-m')\theta]\, 2\pi d\theta \right] \exp - \left\{ \frac{(m^2 - m'^2)v_{th}}{4qR(p\partial\omega_c/\partial\theta)} \right\}^2$$

where the value of the exponentional argument is taken in the cyclotron layer. The last correction introduced by the decreasing exponentional term is only effective for large values of (m,m'), corresponding to a longitudinal scale $\simeq qR/m \simeq (v_{th}/\nabla_{//}p\omega_c)^{1/2}$.

A difficulty that the code has to cope with is linked to the problem of singular modes excited by the compressional field with a structure determined by (3). It is important to understand that excitation in the context of the variational principle. If the finite Larmor radius effect is left apart, the only differentiation $\partial/\partial\psi$ (across the magnetic surfaces) to be performed in the functional $\mathcal{L}(\vec{A},\vec{A}^*)$ appears on $A_\phi(\psi,\theta)$ through the term $|(\nabla\times A)_{//}|^2$ present in $\mathcal{L}_{vac}$. A synthetic expression of $\mathcal{L}$ is :

$$\mathcal{L} = \int d\psi \int \{|G|^2 + (\mathbb{P}A_1)A_1^* + (\mathbb{P}'A_2)A_2^* + (\mathbb{P}''A_2)A_1^* + (\mathbb{P}'''A_2)A_1^*\} d\theta \quad (8)$$

where $G(\psi,\theta) = (\nabla \times A)_{//}$ takes the form:

$$G = \frac{\partial A_2}{\partial \psi} + \mathbb{Q}A_1 + \mathbb{Q}'A_2$$

$\mathbb{P}$, $\mathbb{P}'$, $\mathbb{P}''$, . . , $\mathbb{Q}$, $\mathbb{Q}'$ being operators acting upon the structure in θ of $A_1(\psi,\theta)$ or $A_2(\psi,\theta)$, for a given ψ value. For a WKB structure along θ the operator $\mathbb{P}$ is identical to $P(\psi,\theta,K_{//})$ defined by (3). The set of Euler's equations derived after minimisation of the functional form $\mathcal{L}$ with respect to A_1^* and A_2^* allows to write:

$$\frac{\partial A_2}{\partial \psi} = G - \mathbb{Q}A_1 - \mathbb{Q}'A_2$$

$$\frac{\partial G}{\partial \psi} = \mathbb{Q}'G + \mathbb{P}'A_2 + \mathbb{P}'''A_1 \qquad (9)$$

$$\mathbb{P}A_1 = -\mathbb{P}''A_2 - \mathbb{Q}G$$

It is clear that the singularity occurs on the magnetic surface where the operator $\mathbb{P}$ degenerates. It is fundamental for this physical structure to be preserved by the processus of discretisation introduced in the numerical code (cf.§IV.3).

As stated above the singular modes excited by the compressional field must be selectively damped when their scale approaches the mesh size. This is made possible in ALCYON by adding to $\mathcal{L}$ a functional form $\mathcal{L}_{Stab}(\vec{A},\vec{A}^*)$ of the form:

$$\mathcal{L}_{Stab} \approx i\, \mathrm{Sgn}(\omega)\, |\Delta P| \iiint d_3\vec{x} \sum_{\varepsilon} \left\{ \left| \frac{\partial^2 A_\varepsilon}{\partial \psi^2} h_\psi^2 \right|^2 + \left| \frac{\partial^2 A_\varepsilon}{\partial \theta^2} h_\theta^2 \right|^2 \right\}$$

where h_ψ, h_θ represent the mesh size along ψ, θ, $\varepsilon=1,2$ and ΔP is given by:

$$\Delta P \approx \frac{\mathcal{R}e(\mathcal{L}(\vec{A},\vec{A}^*))}{\iiint |\vec{A}|^2 d_3\vec{x}} \approx \mathrm{Max}\left(\frac{\omega^2}{c^2}, \frac{\omega^2}{c_A^2}, \frac{N^2}{R^2}\right)$$

In view of (4), the positive quantity $2\omega\,\mathcal{I}m(\mathcal{L}_{Stab})$ is the power artificially damped out from the RF field. It represents the power carried away by the converted waves. The damping due to $\mathcal{L}_{Stab}$ acting on a field component of scale K^{-1} is very weak if $Kh \ll 1$, where h represents the mesh size, because then $\mathcal{I}m(\mathcal{L}_{Stab})/\mathcal{R}e(\mathcal{L}) \simeq (Kh)^4$. On the contrary, $\mathcal{L}_{Stab}$ introduces a strong damping: $\mathcal{I}m(\mathcal{L}_{Stab})/\mathcal{R}e(\mathcal{L}) \simeq 1$, as soon as $Kh \simeq 1$.

IV Field representation and numerical stability problems

In the numerical code Alcyon, the field $A_1(\psi,\theta)$, $A_2(\psi,\theta)$ is represented by its components $A_{\varepsilon k m}$, $\varepsilon = 1,2$, over a suitable basis chosen as Fourier harmonics (m) in the poloidal direction θ and as window type functions (k) along ψ. The functional form $\mathcal{L}$ appears in the code as a discretised bilinear functional form in $A_{\varepsilon k m}, A^*_{\varepsilon\, km}$. The discretised equations are obtained by extremalisation of $\mathcal{L}$ in $A^*_{\varepsilon\, km}$. Obviously at scale larger than the mesh size, the discretised form fulfills the requirement of being very close to the physical one in order to provide an accurate modelisation. However, in practice , it is not possible to satisfy such condition at the mesh scale. This poses a problem of numerical stability already encountered in MHD computations [13].The principle for numerical stability states that at small scales the discretisation process does not give rise to resonant solutions which have no physical counterpart. This imposes that at small scales the numerical $\mathcal{L}$ becomes degenerate only together with the physical $\mathcal{L}$. Equivalently, the two functional forms must exhibit values which, even if they are not equal, are however of the same order .

IV.1 Field representation

The components A_1, A_2 of the RF field are Fourier analysed along θ and developed on a basis of window functions $P_{1k}(\psi)$ for A_1 (resp. $P_{2k}(\psi)$ for A_2) , the index k labeling a set of magnetic surfaces:

$$A_\varepsilon(\psi,\theta) = \sum_k \sum_{m=-M}^{M} A_{\varepsilon km} P_{\varepsilon k}(\psi) \exp(im\theta)$$

where $A_{\varepsilon km}$ is the field component of A_ε in the basis $P_{\varepsilon k}(\psi) e^{im\theta}$. The choice of the basis $P_{\varepsilon k}(\psi)$ is crucial in order to guarantee the numerical stability, i.e. to prevent the occurence of non physical oscillations of the field. We have chosen:

$$P_{1k}(\psi) = \chi_k(\psi),\ P_{2k}(\psi) = 1/2\ \{\ \chi_k(\psi) + \chi_{k-1}(\psi)\ \}$$

$$\frac{d}{d\psi} P_{\varepsilon k}(x) = \frac{\chi_{k-1}(\psi)}{(\psi_k - \psi_{k-1})} - \frac{\chi_k(\psi)}{(\psi_{k+1} - \psi_k)} \tag{10}$$

the function $\chi_k(x)$ is equal to unity in the interval $\psi_k \leqslant \psi \leqslant \psi_{k+1}$ and zero elsewhere. For $\psi_k \leqslant \psi \leqslant \psi_{k+1}$, then: $A_{1m}(\psi) = A_{1km}$, $A_{2m}(\psi) = (A_{2km} + A_{2k+1m})/2$ and $\partial A_{\varepsilon m}(\psi)/\partial\psi = (A_{\varepsilon k+1m} - A_{\varepsilon km})/(\psi_{k+1} - \psi_k)$.

IV.2 Numerical stability

Oscillations at small scale along ψ are susceptible of a WKB representation which is expressed as the following: in the physical case we can write locally $A_{\varepsilon m}(\psi) = \overline{A}_{\varepsilon m} e^{iK_\psi \psi}$, while in the discretised case this becomes $A_{\varepsilon km} = \overline{A}_{\varepsilon m} e^{ik\delta\varphi}$, where $\delta\varphi$ is a constant phase jump between adjacent k-surfaces. For a given field representation, there exists a discretised dispersion relation $\mathcal{D}'(\delta\varphi)=0$ determining the phase jump $\delta\varphi$, in place of the physical dispersion relation $\mathcal{D}(K_\psi)=0$, determining K_ψ. The numerical stability is insured if, when $\mathcal{D}(K_\psi)=0$ does not admit a real solution K_ψ, then there is no real $\delta\varphi$ solution of $\mathcal{D}'(\delta\varphi)=0$. This is indeed equivalent to state that values of the physical and the discretised functional forms are of the same order at small scales.

For sake of clarity ,we illustrate this principle with a simplified version of the functional form $\mathcal{L}$, namely, the vacuum functional form in a cylindrical circular geometry, enabling to study each mode $e^{im\theta}$ separately. The physical expression of $\mathcal{L}$ reduces to:

$$\mathcal{L}(\vec{A},\vec{A}^*) = \int \left[\left| \frac{\partial(rA_2)}{r\partial r} - \frac{im}{r}A_1 \right|^2 + P(|A_1|^2 + |A_2|^2) \right] r dr$$

where $P=-\omega^2/c^2$. Substituting $A_c(r)= \overline{A}_c e^{iK_r r}$ and making $\mathcal{L}$ extremum in $\overline{A}_c^*$ leads to the dispersion relation:

$$P\left[K_r^2 + \frac{m^2}{r^2} + P \right] = 0$$

which exhibits the physical solution $K_r^2 = \omega^2/c^2 - m^2/r^2$. We assume that this solution corresponds to a scale much larger than the mesh scale $h=r_{k+1}-r_k$, i.e., ω^2/c^2 and m^2/r^2 are smaller than the quantity $1/h^2$.

As a first example, the field representation of A_1 and A_2 is taken linear in r over each shell $r_k \leqslant r \leqslant r_{k+1}$: $A_c(r) = A_{ck} + (A_{ck+1} - A_{ck})(r-r_k)/(r_{k+1}-r_k)$. With $A_{ck}= e^{ik\delta\varphi}$, the derivative $\partial A_2/\overline{A}_2\partial r$ in each shell is then equal to iK_r', with $K_r'= 2\sin(\delta\varphi/2)/h$. On the other hand, the average value within each shell of quantities of the form $A_c/\overline{A}_c$ and $|A_c|^2/|\overline{A}_c|^2$ is found to be equal to $\cos(\delta\varphi/2)$ and $\alpha = [1 - 2/3 \sin^2(\delta\varphi/2)]$, respectively. After substitution in $\mathcal{L}$ and extremalisation in $\overline{A}_c^*$, we obtain the discretised dispersion relation :

$$\alpha P\left\{ K_r'^2 + \alpha\left(\frac{m^2}{r^2} + P\right)\right\} + \frac{1}{12} h^2 K_r'^2 \left(K_r' \frac{m}{r} \right)^2 = 0$$

For a given α, this equation is quadratic in $K_r'^2$. It admits for solution $K_r'^2 \simeq \omega^2/c^2 - m^2/r^2$ corresponding to the physical solution K_r^2, but also admits for solution:

$$K_r'^2 = \left(\frac{2\sin(\delta\varphi/2)}{h}\right)^2 \simeq \frac{12\alpha\omega^2/c^2}{h^2 m^2/r^2}$$

The latter corresponds to a real $\delta\varphi$ and therefore to a spurious oscillatory discretised solution when $3\omega^2/c^2 < m^2/r^2$. In fig.3 the analytical solution for a typical case (m =1) is presented as well as the discretised solution obtained from the above representation. We observe the spurious solution for $r < r_0$, $r_0= mc/(\sqrt{3}\,\omega)$.

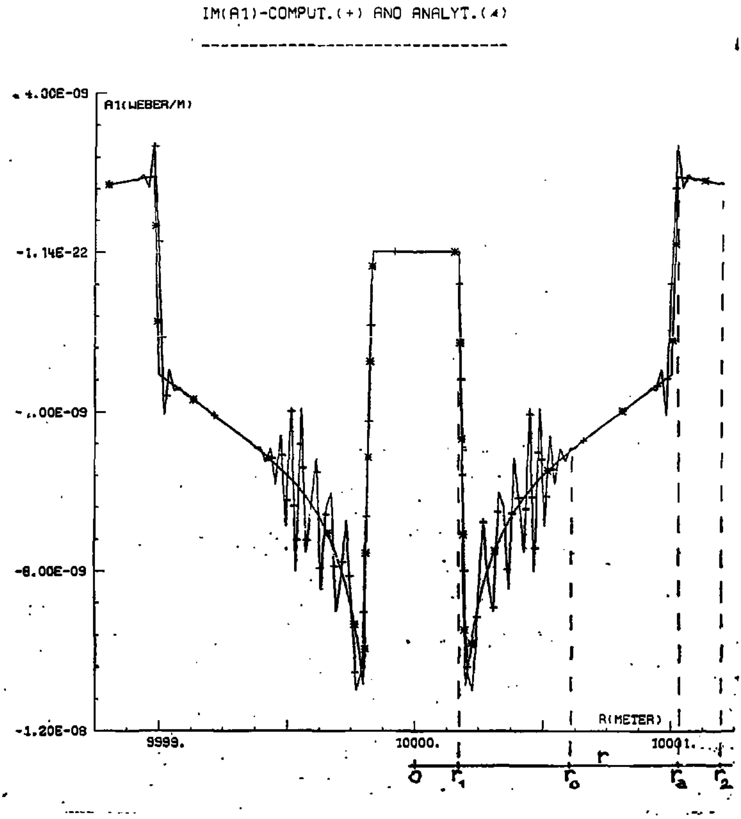

Figure 3

Comparison between the analytical and the discretised solutions for a linear variation of A_1, A_2 over each shell ψ. The magnetic configuration is cylindrical ($r/R = 10^4$, $N_{toroidal} = 10^4$), circular. The soluion $e^{i\theta}$ is computed in vacuum between two nested tori $r = r_1$, $r = r_2$, with the antenna at $r = r_a$. Spurious oscillatory solution is developing for $r < r_0 = c/(\sqrt{3}\,\omega)$.

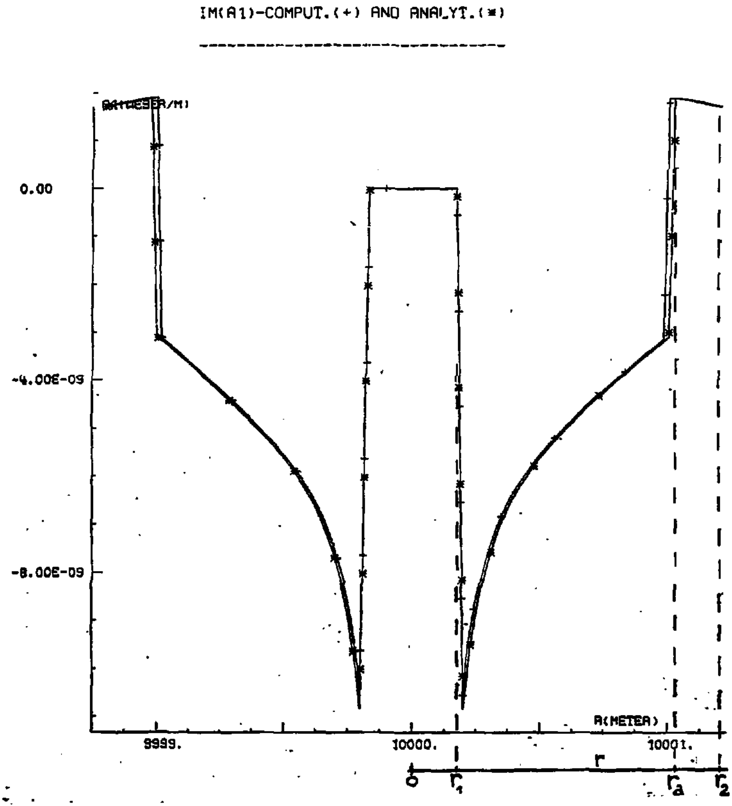

Figure 4

Same as Fig.3 with the representation (10) of the field A_1, A_2.

In general the reason for numerical instabilities lies in the fact that, defining $K_r'(\delta\varphi)$ so that in the average over each shell $|\partial A_2/\partial r|^2 = K_r'^2 |\overline{A}_2|^2$, then the values of $\{\partial A_c/\partial r\, A_c^* / iK_r' A_c A_c^*\}$ and $\{A_c A_c^* / \overline{A}_c\overline{A}_c\}$ are complicated functions of $\delta\varphi$. The discretised dispersion relation is then very different from the physical one and spurious solutions may arise.

The best representation from this point of view is the one where A_1 and A_2 are taken constant on each shell. For instance, taking $A_c(r)=A_{ck}$, $\partial A_c/\partial r = (A_{ck+1} - A_{ck})/(r_{k+1} - r_k)$ leads to:

$$P\left(K_r'^2 + \frac{m^2}{r^2} + P\right) = 0$$

$$\text{with} \quad K_r' = \frac{e^{i\delta\varphi} - 1}{h}$$

which doesn't generate spurious solution . Unfortunately the accuracy is poor. The representation given by eq.10 represents a compromise which has the advantage of a good accuracy and numerical stability.The dispersion relation, in the above simplified case , takes the form:

$$P\left(K_r'^2 + \cos^2\left(\frac{\delta\varphi}{2}\right)\left(\frac{m^2}{r^2} + P\right)\right) = 0$$

$$\text{where} \quad K_r' = \frac{2\sin(\delta\varphi/2)}{h}$$

which is free of spurious solution. This is illustrated in fig.4 for the same set of parameters as fig.3.

IV.3 Torsional resonances

Torsional resonances occur in the physical representation when, on a given ψ surface, the operator $\mathbb{P}$ defined by (8) , acting on the θ structure of A_1, admits a zero eigenvalue. The definition of $\mathbb{P}$ is that $\int(\mathbb{P}A_1)A_1^* d\theta$ gives the term proportional to $A_1A_1^*$ in the functional form $\mathcal{L}$ for the considered surface ψ. After discretisation an operator $\mathbb{P}'$ is built for each shell **k** , which is the correspondent of $\mathbb{P}$. The numerical

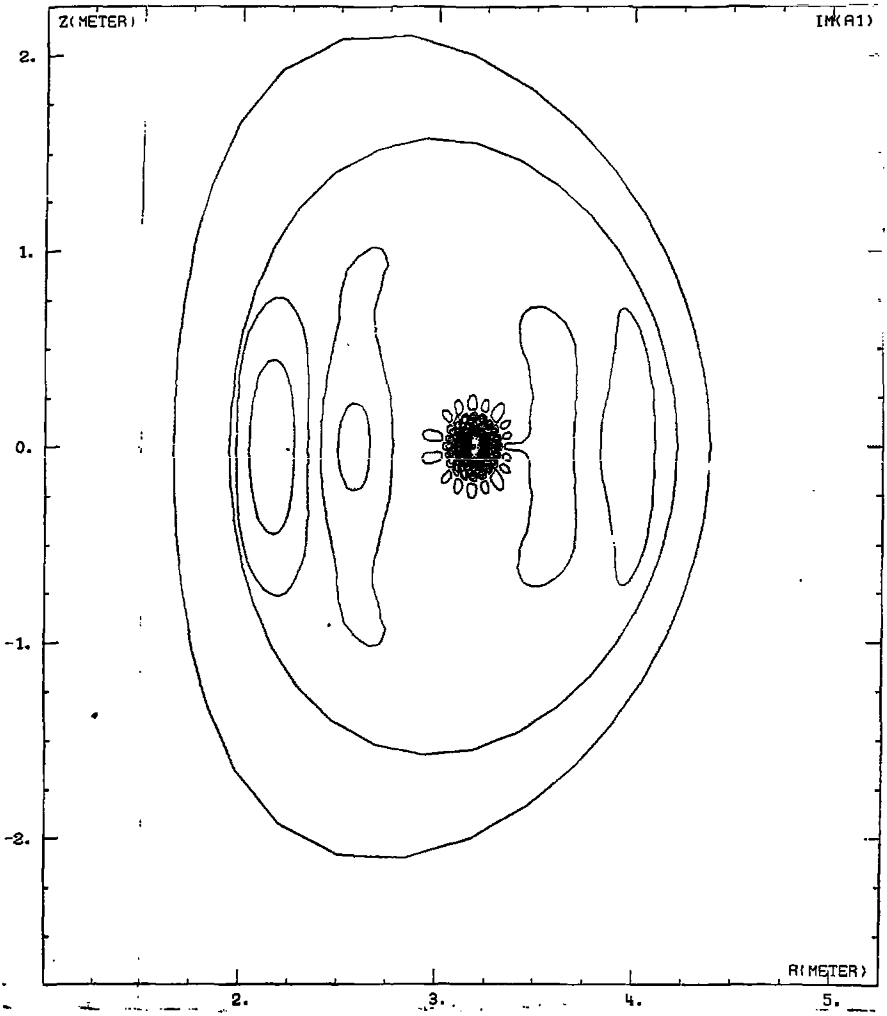

Figure 5a

Effect of the number of Θ harmonics in $(\nabla\times A)_{//}$. This number is here $-20\leftrightarrow 20$, the sum of the number $-10\leftrightarrow 10$ in A_1, A_2 and of the number $-10\leftrightarrow 10$ in the equilibrium parameters. Spurious resonances appear near the centre.

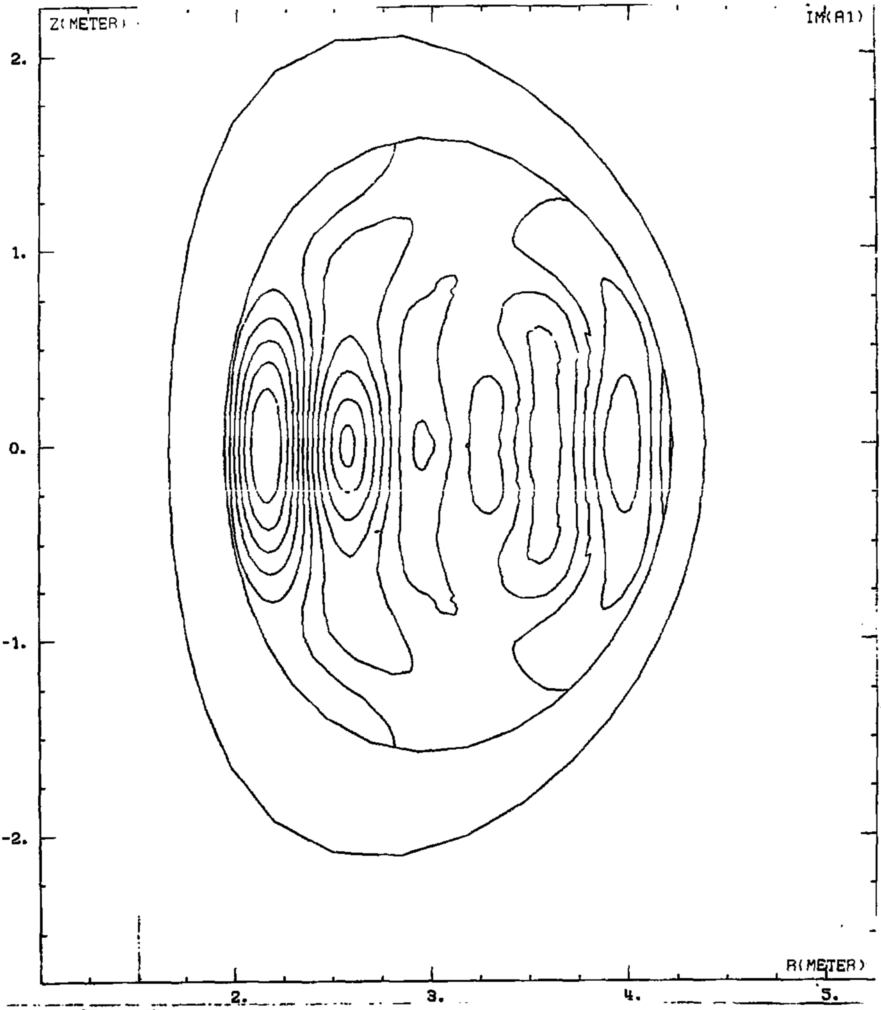

Figure 5b

Same situation as on Fig.5a, but the number of θ harmonics in $(\nabla\times A)_{//}$ is now $-10\leftrightarrow10$, equal to the number in A_1, A_2. The correct field structure is then produced.

stability principle must be respected, i.e., in a given shell, the computation must produce a resonance if, but only if, the discretised operator $\mathbb{P}'$ admits a zero eigenvalue. This is automatically the case if the structure (9) is preserved by the discretisation. One will remark that this structure establishes at each ψ a bijective link between A_1, A_2 and $G=(\nabla x A)_{//}$. In fact, one finds that the structure (9) is preserved if, when modelising the term $\int |G|^2 \, d\theta$ in (8), one introduces G with a discretised structure in θ of the same type as A_1, A_2. In the Alcyon case, this means that G is introduced with the same number of Fourier harmonics in θ as A_1, A_2, by dropping the higher harmonics (they arise because G linearly results from A_1, A_2 with coefficients involving the equilibrium depending on θ). That procedure guarantees the numerical stability even when the computation is performed with a moderate number of θ harmonics. Its effect is demonstrated on the Figures 5a, 5b, which give the map of A_1 in a JET situation, using the θ harmonics $-10 \leq m \leq 10$ for A_1, A_2. Spurious resonances are found when G is introduced in (8) by the harmonics $-20 \leq m \leq 20$ (Fig.5a). The correct field structure is obtained by using for G the harmonics $-10 \leq m \leq 10$ as for A_1, A_2 (Fig.5b).

IV.4 Field regularization on the magnetic axis

In principle the variational principle $\partial \mathcal{L} / \partial A_\ell^* = 0$ should imply the regularity of the field A_1, A_2 on the magnetic axis, because of the presence in $\mathcal{L}$ of diverging terms when the field is not regular. In practice, it has been found necessary to impose the θ structure of A_1, A_2 near the magnetic axis : $A_1, A_2 = \lambda \, (e^{iu}, -ie^{iu}) + \lambda' \, (e^{-iu}, ie^{-iu})$, where λ and λ' are arbitrary constants while the angle u is related to the intrinsic angle $\bar{\theta}$, such that $\nabla_{//} \bar{\theta} / \nabla_{//} \varphi = q(\psi)$, by the formulas:

$$\cos(u) = \cos(\bar{\theta}) \sqrt{\frac{1+c}{1+c \cos(2\bar{\theta})}}$$

$$\sin(u) = \sin(\bar{\theta}) \sqrt{\frac{1-c}{1+c \cos(2\bar{\theta})}}$$

c being related to the excentricity e of the magnetic surfaces in the vicinity of the magnetic axis: $c=(e^2-1)/(e^2+1)$. The effect of that procedure is visible on the Figures 6a, 6b.

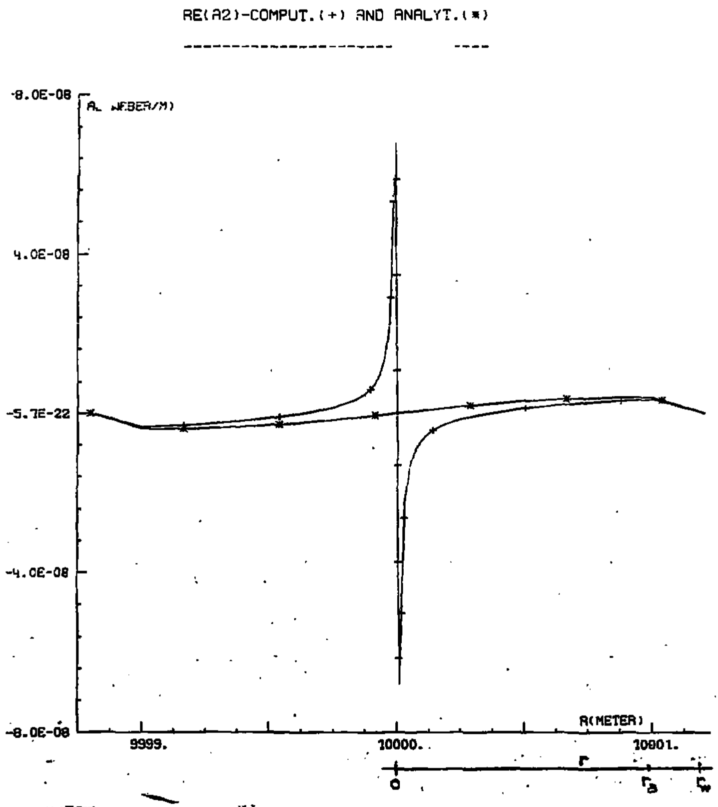

Figure 6a

Comparison of analytical and computed solutions in a cylindrical circular case (m=0 , antenna at $r = r_a$, wall at $r = r_w$) without imposing on the field the θ structure derived from regularity on the magnetic axis.

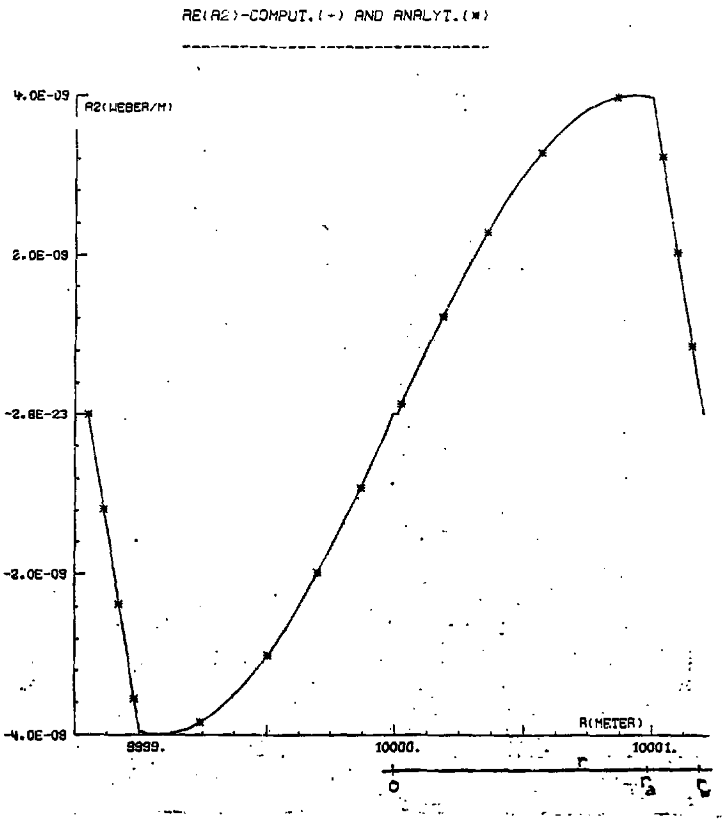

Figure 6b
Same as Fig.6a but imposing now the θ structure derived from regularity on the magnetic axis.

IV.5 The inversion algorithm

The variational principle leads to a vectorial relation MX=F, where the vector X stands for the field components $A_{\varepsilon k m}$ the vector F is deduced from $\mathcal{L}_{Ant}$ and the matrix M is deduced from $\mathcal{L}_{Vac} + \mathcal{L}_{Part} + \mathcal{L}_{Stab}$. The matrix M is pentadiagonal by blocks of dimension $[2(2M+1)]^2$ corresponding to the (2M+1) θ Fourier harmonics $-M \leq m \leq M$ for each of the 2 components A_ε, $\varepsilon = 1,2$. The algorithm chosen to perform the inversion of the matrix M is a direct Gauss factorization allowing to build two block matrices L and U tridiagonal by blocks

$$L = \begin{vmatrix} c'_1 & & & & \\ & \ddots & & & 0 \\ & a'_k & b'_k & c'_k & \\ 0 & & & \ddots & \\ & & a'_n & b'_n & c'_n \end{vmatrix} \qquad U = \begin{vmatrix} 1 & d'_1 & e'_1 & & 0 \\ & \ddots & & & \\ & & 1 & d'_k & e'_k \\ 0 & & & \ddots & \\ & & & & 1 \end{vmatrix}$$

such that M=LU. The solution is then obtained by first solving LF'=F and next UX=F'.The factorisation is always possible, without permutation of lines, because the imaginary part of the functional form $\mathcal{L}_{Vac} + \mathcal{L}_{Part} + \mathcal{L}_{Stab}$ which generates the matrix M is definite positive (see eq.4). For 2M+1=81 θ harmonics and K=121 radial shells (the mesh structure used for the computations presented below), the accuracy of the inversion on Cray 1 is $\sim 10^{-12}$. The computation time is 160 s, varying as $K.M^{2.4}$. The quality of the Alcyon output is only limited by the scale of the computed field compared to the mesh size. The results are excellent with 7 shells for a quarter of radial period, as shown by the Figures 7a,7b , and are still reliable with 3 or 4 shells.

V. Analysis of typical RF heating schemes in JET configuration.

In this section we present the ALCYON results for some heating scenarios that

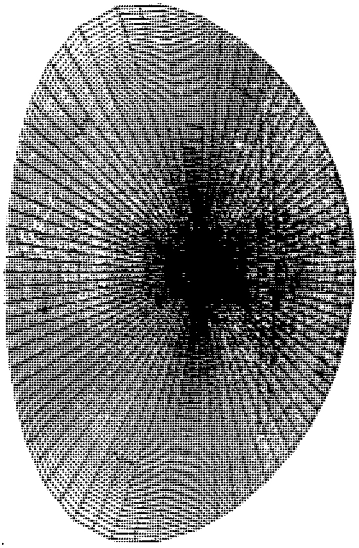

I

121 shells ψ_k, ψ_{k+1}

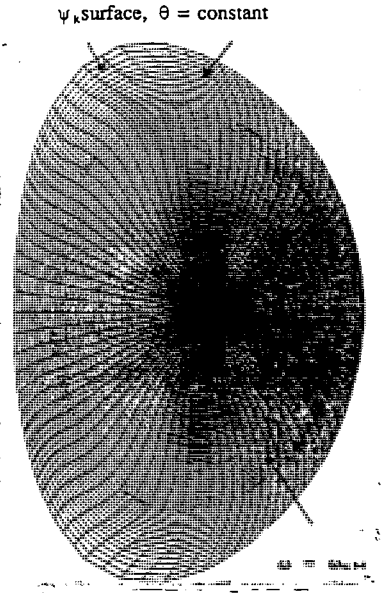

III

121 shells. The $\psi_k$surfaces and the angular coordinate θ chosen to refine the mesh near the resonance $\omega=\omega_{cH}$

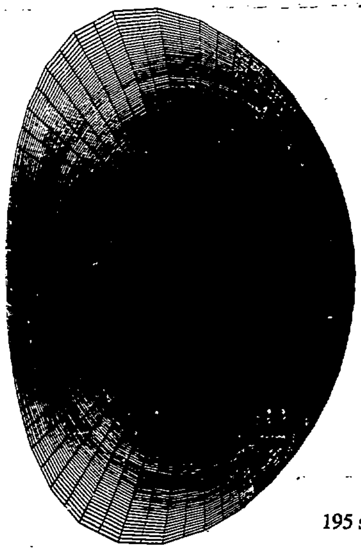

II

195 shells

Figure 7a: mesh structures for a JET configuration.

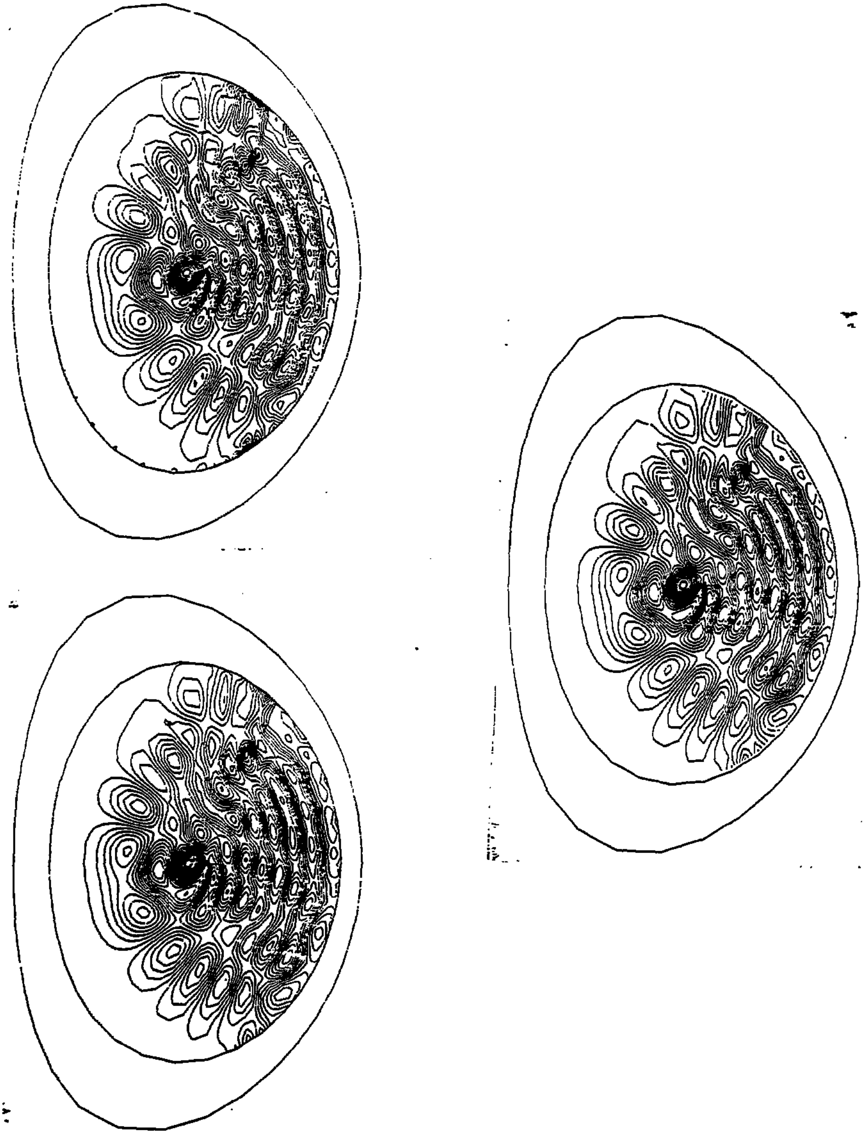

Figure 7b
Computations of the same R.F. field with the mesh I, II, III of Fig.7a.

are under experimental study on JET. We focus on Deuterium plasmas with Hydrogen as minority ions, with ratios n_H/n_D ranging from 0%, 5% to 20% in order to review the effect of second and first harmonic heating as well as mode conversion. The main plasma parameters are: $T_e = T_H = T_D = 5$ keV, $n_e = 10^{20}$ m^{-3} or 0.25 10^{20} m^{-3}, I_p= 2 MA, B_T = 2.3 T. The RF frequency $f = \omega/2\pi$ is 33 or 29 MHz, locating the cyclotron resonance layer ($\omega = \omega_{cH} = 2\omega_{cD}$) at the plasma centre or at mid radius outwards. Both the density and temperature profiles are flat and vary like $(1-\overline{\psi}^2)^{1/2}$ where $\overline{\psi} = (\psi-\psi_A)/(\psi_{PB}-\psi_A)$, "A" standing for axis and "PB" for plasma boundary. The JET magnetic configuration and the RF antenna extension are presented in Fig.7 .

V.1 Stochastic behaviour and second harmonic heating

We here consider the case of a pure Deuterium plasma. For f = 33 MHz, the second harmonic resonance of the deuterium should occur near the plasma centre, but is disaccounted in first place (Fig.8). The bulk perpendicular wavenumber ω/C_A is 70 m^{-1} and the corresponding wavelength 9 cm. The mesh size being 1 cm the Nyquist criteria is well respected and there is no aliasing problem in the field picture. We observe then that the field fills up all the plasma with a stochastic structure which, as regular as it may appears, changes totally for a slight variation of the boundary conditions. If the second harmonic resonance is introduced (Fig.9) then the field structure is dramatically alterated: we have a well focussed wave nearly absorbed by the resonance in a single pass. There is little to no small scale structure developing in the resonance zone which shows that the mode conversion process occuring near the resonance is negligeable. The absorbed power peaks at a radius of 0.2 m and extends to 30 cm in total. This is consistant with the Döppler width $\simeq \pm$ 10 cm for a toroidal N number of 30, taking into account that the power deposition profile is the result of the convolution of the number of ψ surfaces intersected by the resonance layer and of the Döppler width.

V.2 Minority heating scenario

The hydrogen density is now raised to 5% and the second harmonic resonance of Deuterium ions is not introduced. For f = 33 MHz, the surface and the mode conversion surface P=0 are passing close to the centre. Observing the field structure (Fig.10) we note, as in the case of second harmonic heating, that the wave is well focussed and absorbed in one pass. One may also verify from the map of $|\tilde{A}|$ that the magnetosonic

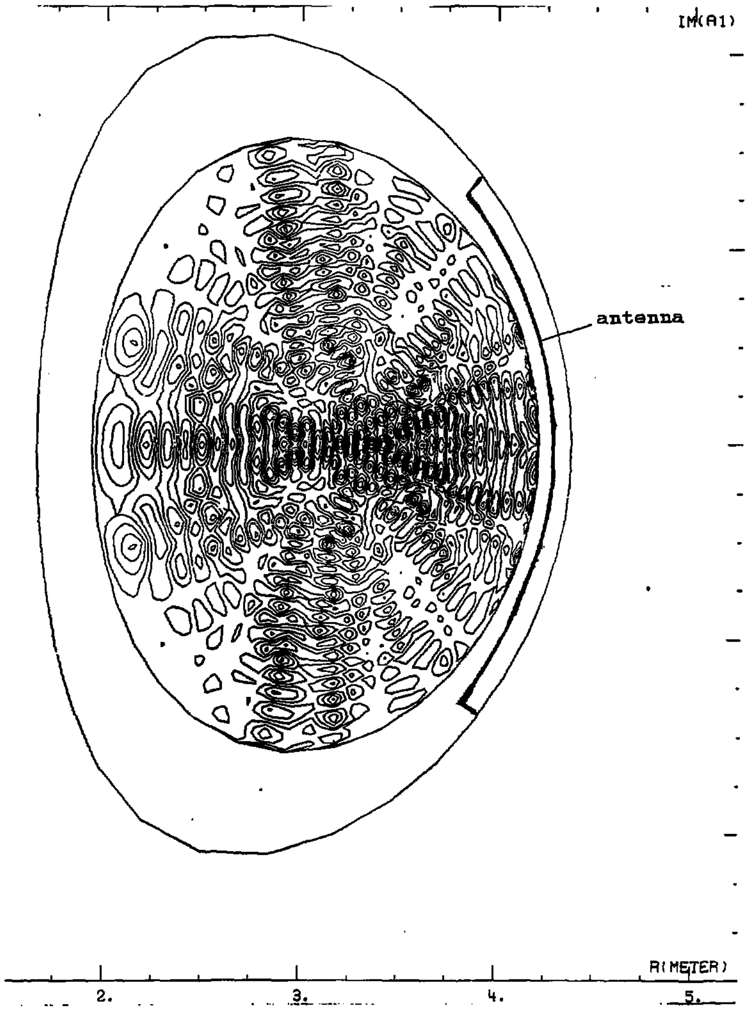

Figure 8

Map of A_1 in a case of stochastic behaviour: pure D plasma without power absorption.

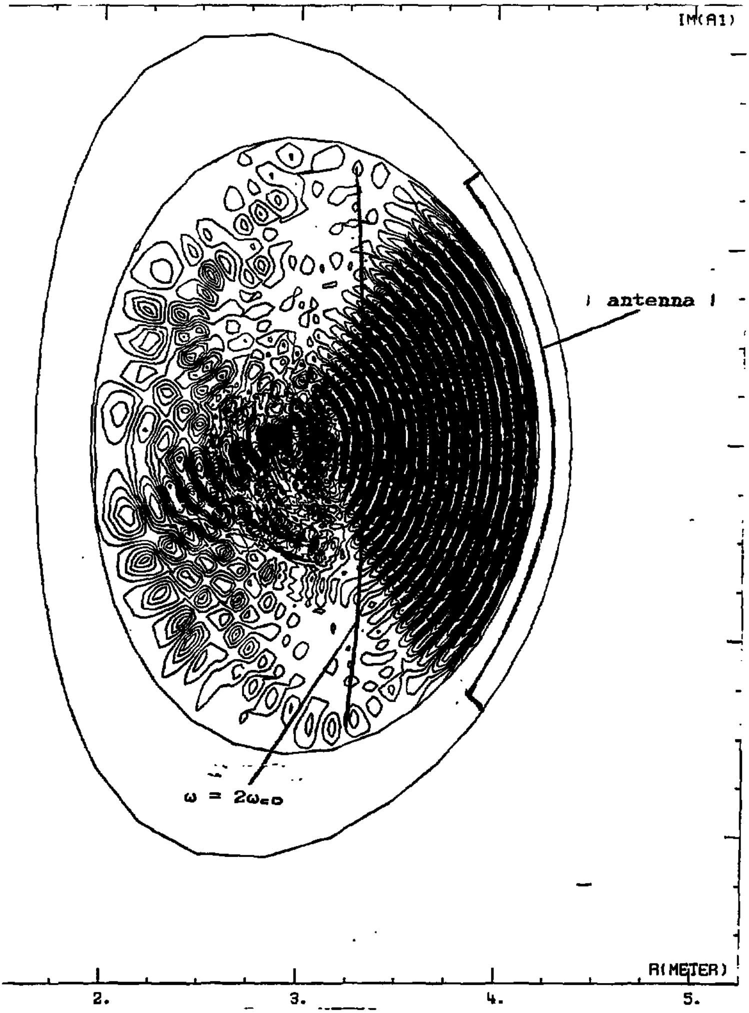

Figure 9

Same as Fig.8, but with second harmonic absorption of D ions included.

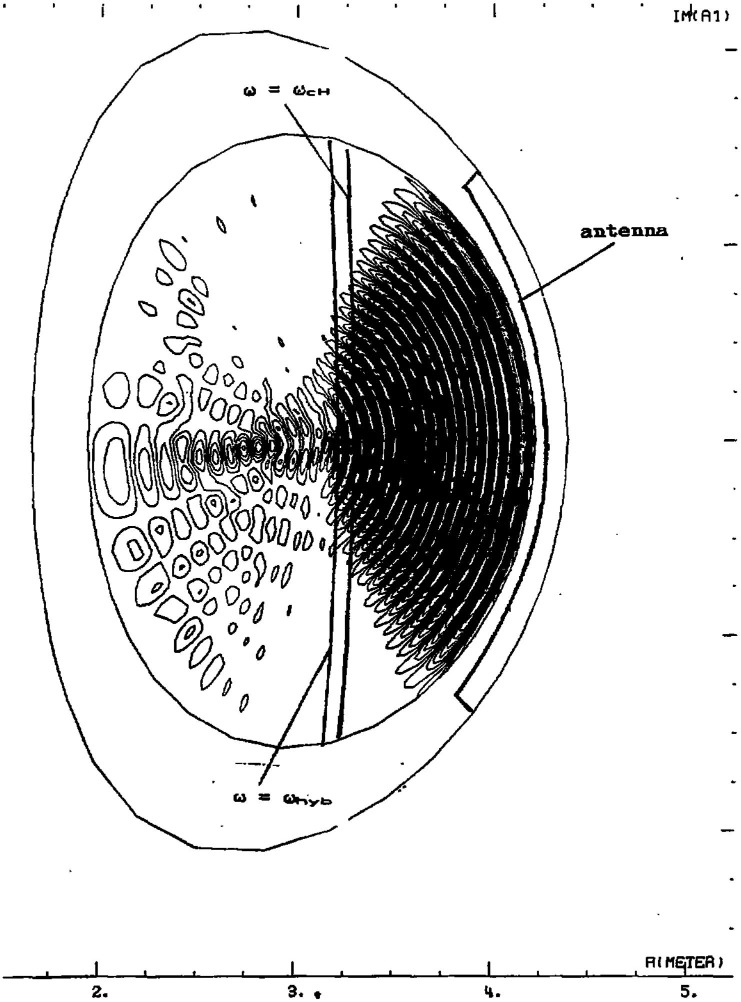

Figure 10

Same as Fig.9, removing second harmonic absorption by D ions, introducing minority absorption by H ions: n_H/n_D=5%; N=30.

wave is travelling on the low field side of the cyclotronic resonance and strongly damped down in its vicinity. The mode conversion is not apparent on the field structure because the Döppler width $\simeq \pm 15$ cm covers the conversion zone.

V.3 Observation of the hybrid resonance

When N is reduced the Döppler width lessen proportionally and one expects to observe a small scale structure developing, even for a small n_H/n_D of 5%. To clarify the phenomenon the RF frequency is decreased to 29 MHz, shifting the cyclotron and the hybrid resonance outwards. When N=30 (Fig.10a) the field structure has the same structure as in case V.2, with an absorption smoothly spread over the Döppler width (Fig.11b). Switching to N=5 (Fig.12a) one observes a stationary pattern of the wave on the low field side of the resonance, and an amplification of the field around the hybrid layer. The power, although mainly deposited in the vicinity of the cyclotronic resonance, is sensitive to the field pattern and in particular a noticeable absorption continues to take place near the hybrid layer (Fig.12b). In this case however the total absorbed power is reduced and does only reached 0.178 MW instead of 0.206 MW for N = 30.

V.4 Low field side vs. high field side excitation. Mode conversion heating.

So far, as n_H/n_D=5%, it has not been necessary to damp out the small scale wave excited around the mode conversion layer, as the broadening of the cyclotron resonance was allowing the computation to deal with the hybrid singularity. This is no longer possible when n_H/n_D=20%. Then to reach a sensible result the small scale modes need to be damped down by the functional form $\mathcal{L}_{stab}$. We have further reduced the density to $0.25\ 10^{20}\ m^{-3}$ resulting in doubling the wavelength and put N=15.

In case of an outside launch, the field structure is stationary on the low field side of the hybrid resonance. It is noticeable (Fig.13a) that the field actually extends up to the hybrid layer and is not strongly reflected at the cutoff (located at roughly two third of the distance separating the cyclotron and the hybrid resonance). This may be understood as the wavelength is of order of the distance separating the cutoff from the hybrid resonance. One may also remark that the stationary structure results in more than doubling the amplitude of the field by comparison with the case V.3. The total power deposited for the same antenna current reaches 0.782 MW compared to 0.206 MW. The power deposition profile presents a

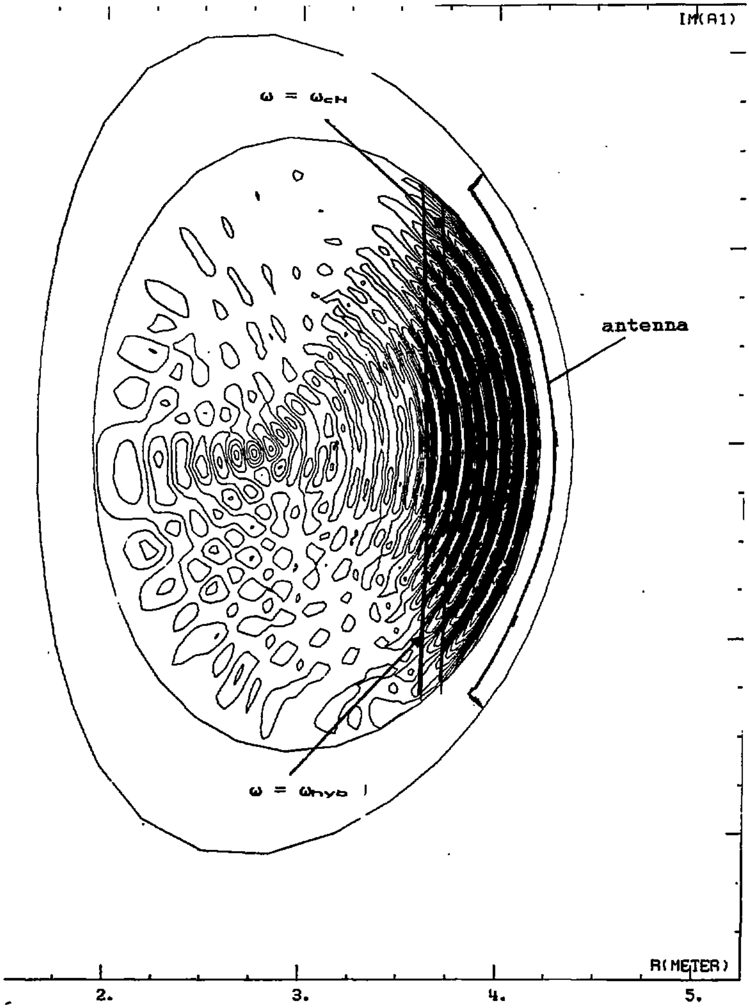

Figure 11a

Same as Fig.10, but with a R.F. frequency of 29 MHz.

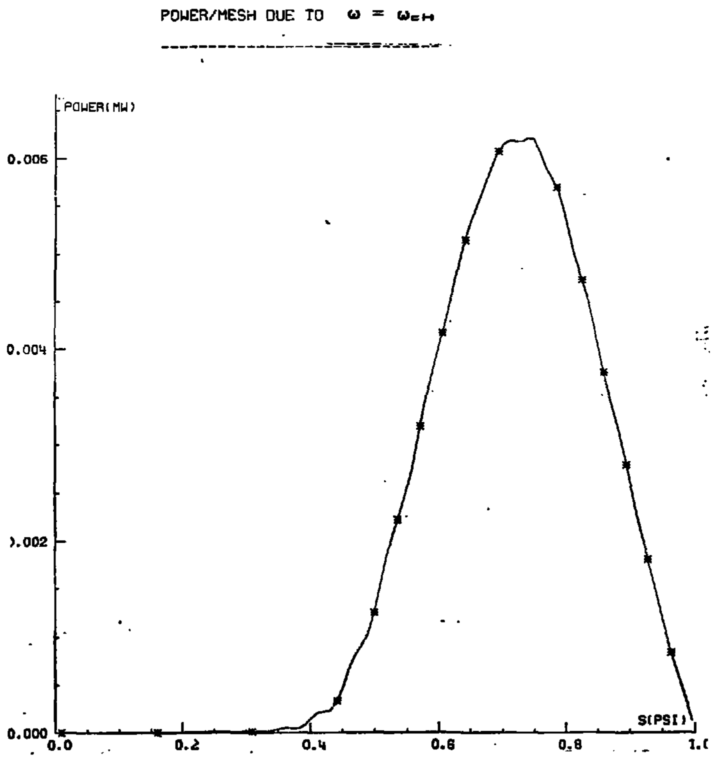

Figure 11b
Averaged power deposited on each ψ surface (mag. axis $\leftrightarrow$ s=0; plasma edge $\leftrightarrow$ s=1) for Fig.11a case.

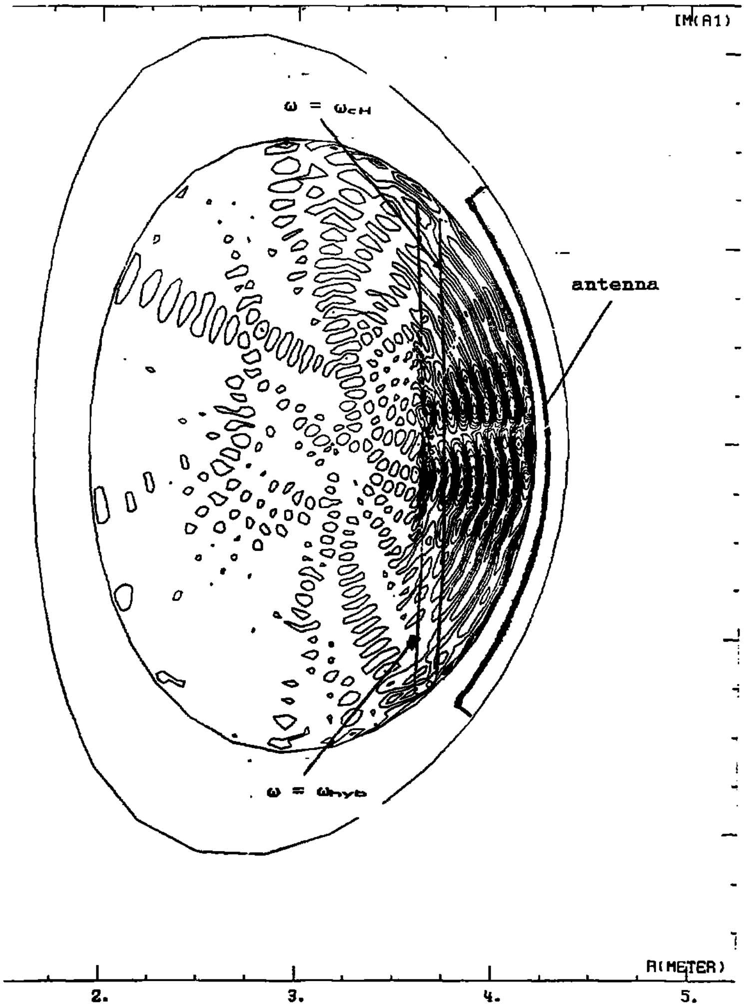

Figure 12a
Same as Fig.11a, but with N=5.

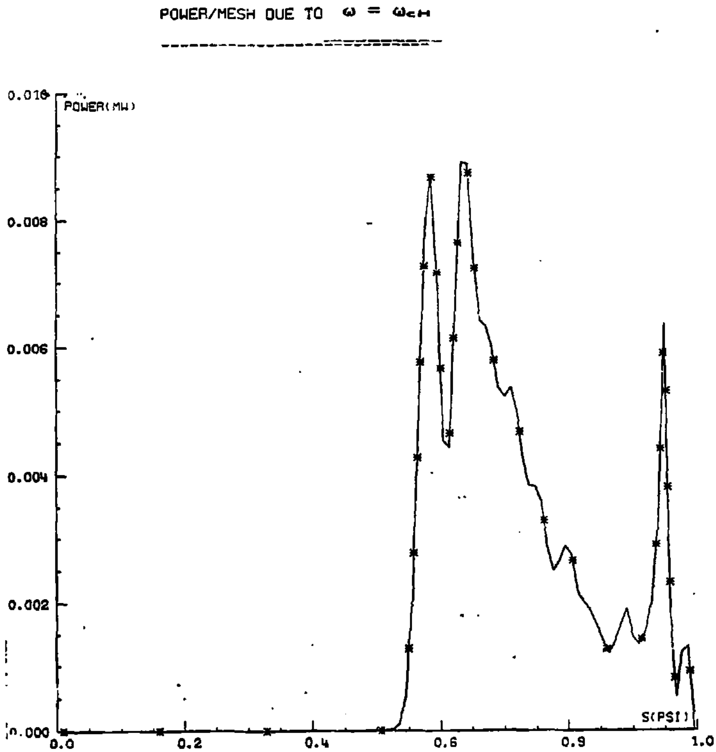

Figure 12b

Averaged power deposited on each ψ surface for the case of Fig.12a.

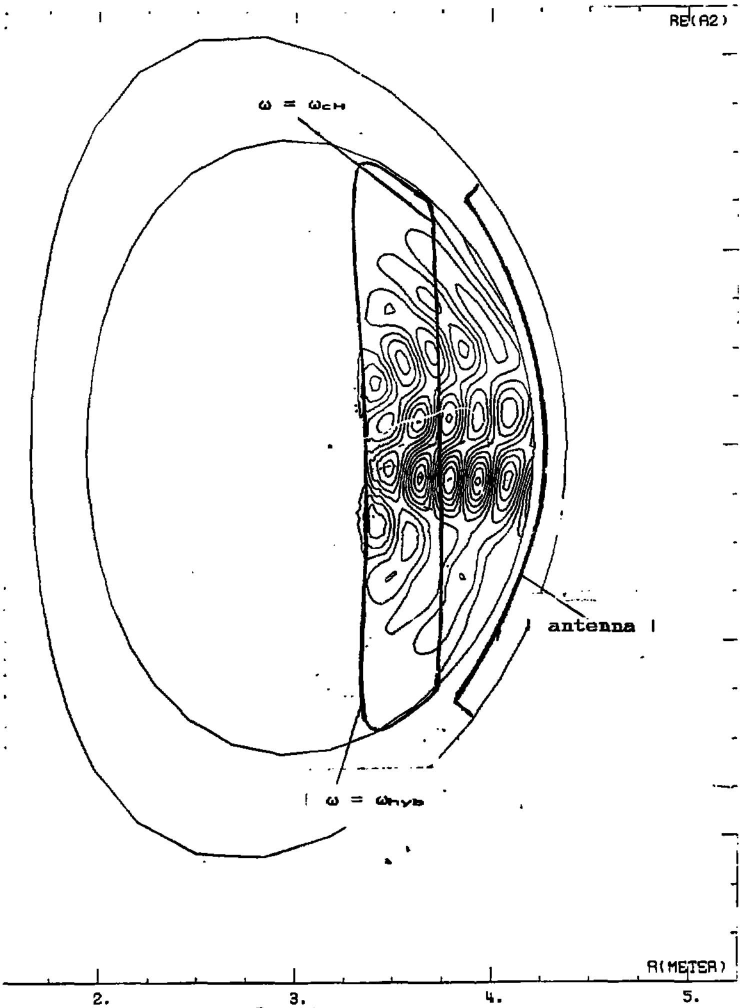

Figure 13a
Map of A_2 for n_H/n_D=20%, N=15, outside launch.

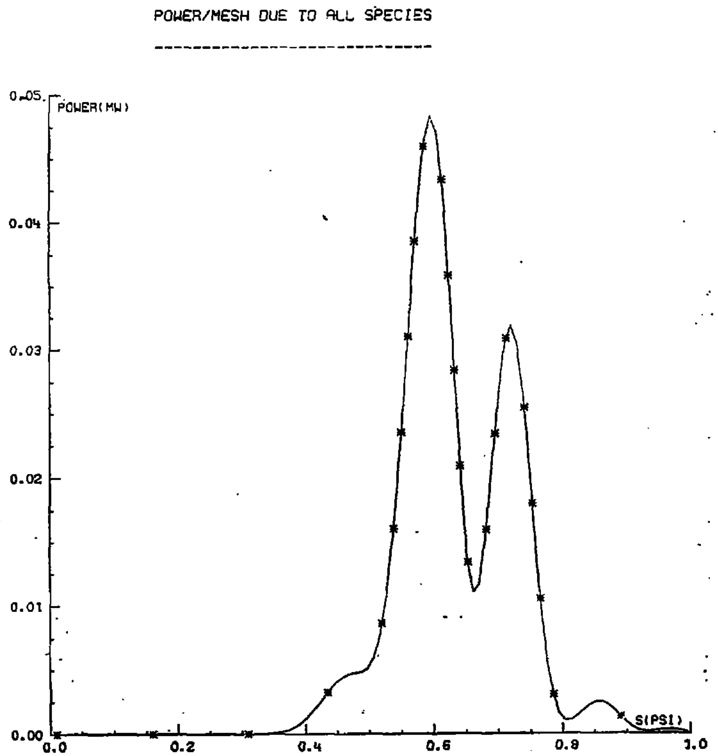

Figure 13b

Averaged power deposited on each ψ surface for the case of Fig.13a. The absorption is all due to the cyclotron resonance, the contribution of the stabilisation functional form being negligible.

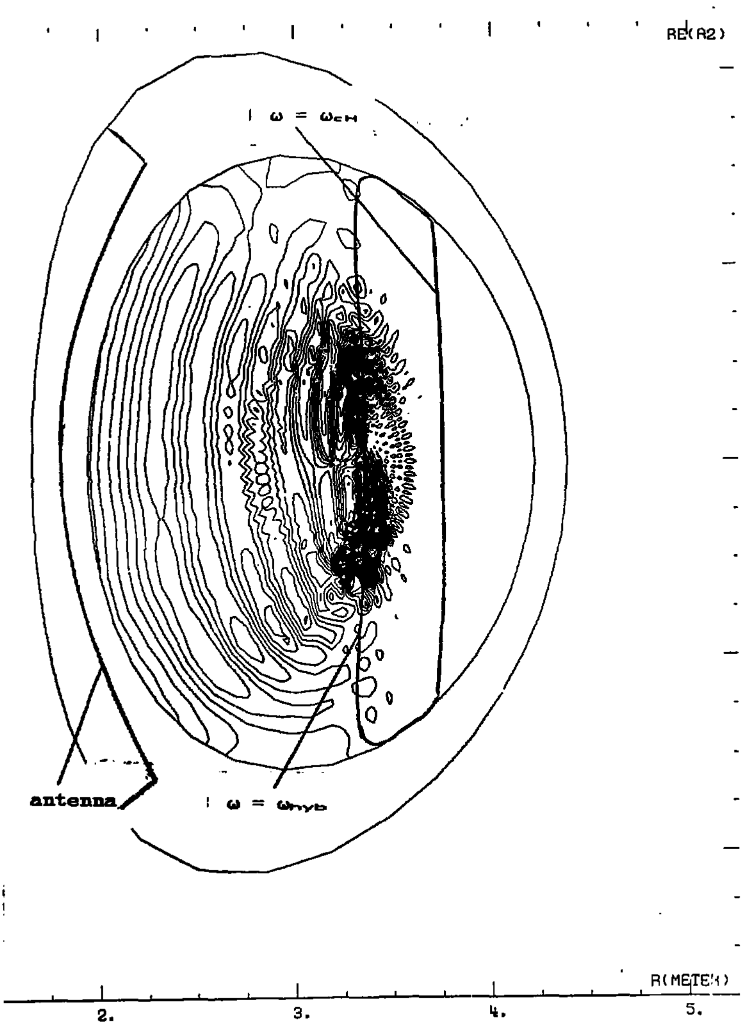

Figure 14a
Same as Fig.13a, but for an inside launch.

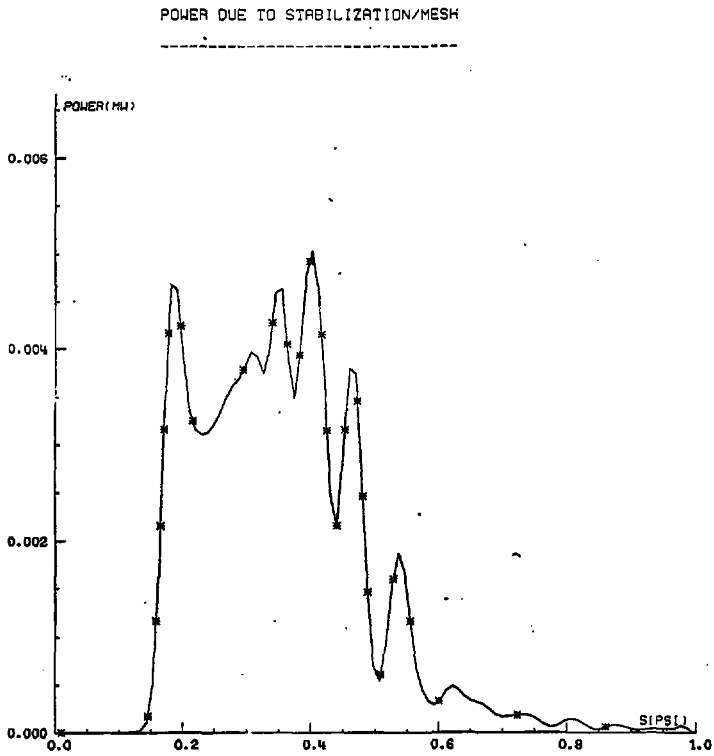

Figure 14b

Averaged power deposited on each ψ surface for the case of Fig.14a. the absorption is here due to the stabilization functional form (the same form as in the case of Fig.13a,b), with a negligible contribution of the cyclotron resonance.

dip at the location of the cyclotron resonance (Fig.13b). One recognises here the plasma shielding effect when the minority concentration is high. The power absorption is due to the cyclotron resonance effect, while the stabilising power is negligible.

For the inside launch with an equivalent antenna length in θ, the magnetosonic wave runs first into the hybrid resonance (Fig.14a). The structure of the field is regular on the high field side of the hybrid resonance and is strongly amplified around it. A fine scale structure compatible with the mesh scale is excited on the hybrid surface and produces a stationary field structure along θ visible only on the low field side.Such structures have been seen with the code LION [14 -15], but in our case they exist only on surfaces ψ which do not intercept the resonance layer $\omega = \omega_{cH}$. Apart from the torsional modes the field does not reached the low magnetic field side of the plasma. The power deposited is here entirely due to the effect of the stabilisation functional form, and reaches 0.156 MW. The deposition profile is broad (40 cm), starting at the hybrid layer location (Fig.14b).

VI. Conclusions

In this report, the numerical code "ALCYON" based on a variational formulation of the ICRF problem has been presented: that code is characterised by the possibility to take into account thermal and inhomogeneity effects, to refine the mesh structure around the cyclotron and conversion resonance layers and to cancel out selectively the modes of radial structure reaching the mesh size. Furthermore suitable discretisation process has been implemented avoiding the developement of spurious oscillatory solutions and producing as accurate solutions as possible. A number of possibilities for errors have been successfully tested in ad hoc cases where the solution could be compared to the analytical one.

Put at work in realistic ICRF heating cases, ALCYON handles most of the physical phenomenons of absorption and resonances, from stochastic field behaviour in the no absorption case, up to mode conversion onto small scale Bernstein waves. The only limit is the need of a number of mesh points large enough for the magnetosonic wavelength to be correctly represented. The obtained results give ALCYON the credibility to undertake a systematic study of those phenomenons - which indeed has been started- and to be regarded as an accurate predicting code for ICRF experiments. Further development are foreseen which could allow to handle the ICRF thermal emission and give a better representation of the RF field near the antenna system. Finally, when coupled to a Fokker-Planck code, ALCYON should prove to be a useful tool to tackle the high energy population evolution during ICRH.

Acknowledgements: The support of D.F Duchs and T. Hellsten is gratefully acknowledged. This work has been developed under the Article 14 of the JET status contract Nb JT5 9003.

References

[1] Adam J., Plasma Physics and Controlled Fusion 29 (4) 1987, p.443.

[2] Gambier D.J., Samain A., Nucl. Fusion 25 (3) 1985, p.283.

[3] Brambilla M., IPP Rep. 5/10 1986, Garching (Germany).

[4] Swanson D.G., Phys. Fluids 28 (9) 1985 p.2645 (references therein).

[5] Gambier D.J., Schmidt J.P.M., Phys Fluids 26 (8) 1983, p.2200.

[6] Budden K.G., "The propagation of radio waves", Cambridge University Press, Cambridge 1985.

[7] Itoh K., Itoh S.I., Fukuyama A., Nucl. Fusion 24 (1984) p.13.

[8] Smithe D.N., Colestock P.L., Kashuba R.J., Kammash T., PPPL Rep. 2400 (1987) Princeton University, Princeton N.J. (U.S.A).

[9] Villard L., Appert K., Gruber R., Vaclavich J., CRPP Rep. 275/85, Ecole Polytechnique Federale de Lausanne (Switzerland).

[10] Adam J., Samain A., Rep. Euratom CEA FC 579 (1971), CEN Fontenay Aux-Roses (France).

[11] Perkins F.N., Nucl. Fusion 17 (1977) p.1197.

[12] Stix T.H., Swanson D.G., "Handbook of Plasma Physics", edited by A. Galeev and R.N. Sudan (North-Holland, Amsterdam, 1983), Vol. 1 p.335.

[13] Gruber R., Rappaz J., Finite Element Method in Linear Ideal Magnetohydrodynamics (Springer-Verlag, Berlin-Heidelberg,1985).

[14] Hellsten T., Appert K., Proc. of the 13th European Conf. on Controlled Fusion and Plasma Heating, Schliersee, Germany (1986) Vol. Pt.II, p.129.

[15] Villard L., PHD Thesis (1987), Ecole Polytechnique Federale de Lausanne (Switzerland).